Cytosolic γ-Glutamyl Peptidases Process Glutathione Conjugates in the Biosynthesis of Glucosinolates and Camalexin in *Arabidopsis* [W][OA]

Fernando Geu-Flores,[a,b,1,2] Morten Emil Møldrup,[a,b,2] Christoph Böttcher,[c] Carl Erik Olsen,[d] Dierk Scheel,[c] and Barbara Ann Halkier[a,b,3]

[a] Section for Molecular Plant Biology, Department of Plant Biology and Biotechnology, Faculty of Life Sciences, University of Copenhagen, 1871 Frederiksberg, Denmark
[b] Villum Kann Rasmussen Research Centre for Pro-Active Plants, Department of Plant Biology and Biotechnology, Faculty of Life Sciences, 1871 Frederiksberg, Denmark
[c] Department of Stress and Developmental Biology, Leibniz Institute of Plant Biochemistry, 06120 Halle/Saale, Germany
[d] Department of Natural Sciences, Faculty of Life Sciences, University of Copenhagen, 1871 Frederiksberg, Denmark

The defense-related plant metabolites known as glucosinolates play important roles in agriculture, ecology, and human health. Despite an advanced biochemical understanding of the glucosinolate pathway, the source of the reduced sulfur atom in the core glucosinolate structure remains unknown. Recent evidence has pointed toward GSH, which would require further involvement of a GSH conjugate processing enzyme. In this article, we show that an *Arabidopsis thaliana* mutant impaired in the production of the γ-glutamyl peptidases GGP1 and GGP3 has altered glucosinolate levels and accumulates up to 10 related GSH conjugates. We also show that the double mutant is impaired in the production of camalexin and accumulates high amounts of the camalexin intermediate GS-IAN upon induction. In addition, we demonstrate that the cellular and subcellular localization of GGP1 and GGP3 matches that of known glucosinolate and camalexin enzymes. Finally, we show that the purified recombinant GGPs can metabolize at least nine of the 10 glucosinolate-related GSH conjugates as well as GS-IAN. Our results demonstrate that GSH is the sulfur donor in the biosynthesis of glucosinolates and establish an in vivo function for the only known cytosolic plant γ-glutamyl peptidases, namely, the processing of GSH conjugates in the glucosinolate and camalexin pathways.

INTRODUCTION

Among the most well-studied defense-related compounds in plants is the group of metabolites known as glucosinolates. Glucosinolates are sulfur-containing secondary metabolites characteristic of the order Brassicales, which includes the agriculturally important oilseed rape (*Brassica napus*), the cruciferous vegetables, and the model plant *Arabidopsis thaliana* (Fahey et al., 2001). Together with the enzyme myrosinase, glucosinolates constitute the so-called mustard oil bomb, which is a binary defense system against generalist insects (Hopkins et al., 2009) and has also been implicated in defense against nonadapted pathogens (Bednarek et al., 2009; Clay et al., 2009). Apart from their ecological and agricultural importance, glucosinolates have been proposed to have cancer-preventive properties (Higdon

et al., 2007; Hayes et al., 2008), which has sparked great interest in their metabolic engineering and heterologous production (Gasper et al., 2005; Geu-Flores et al., 2009). After a decade of glucosinolate research in the *Arabidopsis* postgenomic era, the biosynthetic pathway is well understood and most biosynthetic genes are known (Sønderby et al., 2010). A notable exception is the step involving the incorporation of reduced sulfur, where the identity of the donating thiol has not been established (Sønderby et al., 2010).
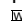
The tripeptide GSH (γ-Glu-Cys-Gly) is the most abundant low-molecular-weight thiol in the cell and is involved in numerous cellular processes, such as redox homeostasis, redox sensing, and detoxification of xenobiotics and heavy metals (Noctor and Foyer, 1998; Cobbett, 2000; Rea, 2007; Meyer, 2008; Rouhier et al., 2008; Pal and Rai, 2010; Cummins et al., 2011). By virtue of the reducing properties of thiols, GSH can detoxify reactive oxygen species either directly (e.g., by quenching free radicals) or indirectly (e.g., via the GSH-ascorbate cycle, which detoxifies H_2O_2 enzymatically) (Noctor and Foyer, 1998; Meyer, 2008). GSH is also involved in the detoxification of heavy metals and xenobiotics, where the strong nucleophilic properties of thiols are exploited biologically. Heavy metals are detoxified by chelation with GSH oligomers called phytochelatins (n = 2 to 11) and the apparently nontoxic organometallic complexes are stored in the vacuole (Cobbett, 2000; Pal and Rai, 2010). In turn, xenobiotics
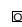
with electrophilic centers are conjugated to GSH either non-enzymatically or by the action of glutathione *S*-transferases (GSTs) (Cummins et al., 2011). The GSH conjugates are shuttled into the vacuole by transporters of the ABC family (Rea, 2007). Once in the vacuole, degradation to the Cys conjugates proceeds via the sequential action of a γ-glutamyl transpeptidase (GGT) and a yet unidentified carboxypeptidase (Grzam et al., 2006; Ohkama-Ohtsu et al., 2007b).

In addition to the proven biological roles of GSH, a role as sulfur donor in the biosynthesis of glucosinolates has been proposed but remains to be proven (Schlaeppi et al., 2008; Geu-Flores et al., 2009; Dixon et al., 2010). Glucosinolates are synthesized from different amino acids (Trp, Phe, or side chain–elongated Met) through the action of at least five enzymes. The two first are cytochromes P450 of the families CYP79 and CYP83, respectively. These convert the amino acids to activated aldoximes that react spontaneously with thiols to form thiol conjugates. For decades, Cys was thought to be the in vivo sulfur donor; therefore, a GST-like enzyme was proposed to catalyze the specific conjugation to Cys. The Cys conjugate is further processed to a glucosinolate by the sequential action of a *C-S* lyase (SUR1), a glucosyltransferase (at least UGT74B1), and a sulfotransferase (SOT16, 17, or 18) (Sønderby et al., 2010).

The first indication of the involvement of GSH in the biosynthesis of glucosinolates came from the analysis of the *phytoalexin deficient2* (*pad2*) mutant plants. The *pad2* mutation was mapped to the *GSH1* gene, which codes for γ-Glu-Cys synthetase, the enzyme that catalyzes the first of two committed steps in the biosynthesis of GSH from its amino acid constituents. Accordingly, leaves of *pad2* plants were shown to accumulate only around 20% of wild-type GSH levels, while the accumulation of Cys was increased 5-fold (Parisy et al., 2007). With respect to glucosinolates, the uninduced foliar levels were unchanged in *pad2* mutants when compared with wild-type plants, but upon elicitation by a generalist insect, the mutants accumulated less glucosinolates (50% of the wild-type levels of both I3M and 4MSB after 24 h of constant challenge by *Spodoptera littoralis*; Schlaeppi et al., 2008). This suggested a link between GSH and glucosinolate biosynthesis; however, given the multifunctionality of GSH, the exact nature of the link remained unclear. A connection implicating redox regulation via the GSH-ascorbate cycle has been regarded as unlikely, since the ascorbate-deficient mutant *vtc1-1* (which has 25% of wild-type ascorbic acid levels) was not affected in glucosinolate levels (Schlaeppi et al., 2008). Attempts to demonstrate the incorporation of ^{35}S-labeled GSH into glucosinolates have been inconclusive because the label also incorporated into Cys, which is the other sulfur donor candidate. In a similar fashion, feeding experiments using ^{35}S-labeled Cys have yielded inconclusive results because of the incorporation of the label into GSH even in the presence of the γ-Glu-Cys synthetase inhibitor buthionine sulfoximine (Schlaeppi et al., 2008).

An indication of the involvement of GSH as direct sulfur donor has come from the de novo engineering of benzylglucosinolate (BGLS) into *Nicotiana benthamiana* (Geu-Flores et al., 2009). When the five known BGLS biosynthetic genes were transiently coexpressed in leaves of *N. benthamiana*, BGLS was produced, but it was accompanied by a related GSH conjugate, *S*-[(*Z*)-phenyl-acetohydroximoyl]-L-glutathione (GS-B), which accumulated to

~80-fold higher levels. In accordance with the original proposal that Cys is the sulfur donor, GS-B might have been produced because of the absence of a Cys-conjugating enzyme and the resulting accumulation of its substrate, which was subsequently detoxified by conjugation to GSH. Alternatively, GS-B could be a true intermediate, and its accumulation might have been due to the absence of a GS-B–processing enzyme. The latter hypothesis led to the discovery of γ-*GLUTAMYL PEPTIDASE1* (*GGP1*), a gene that is strongly coregulated with glucosinolate-related genes in *Arabidopsis* and whose coexpression in *N. benthamiana* minimized the accumulation of GS-B and boosted the production of BGLS ~5-fold. Furthermore, heterologously produced GGP1 was able to catalyze the hydrolytic cleavage of the γ-glutamyl residue of GS-B in vitro (Geu-Flores et al., 2009). Although the BGLS study in *N. benthamiana* suggests that GSH is the sulfur donor and that GGP1 is the GSH conjugate-processing enzyme, experimental evidence is needed to demonstrate this in naturally occurring glucosinolate-producing plants.

The phytoalexin camalexin is another well-studied sulfur-containing plant defense compound in *Arabidopsis*, and the sulfur donor in its biosynthesis was recently shown to be GSH (Su et al., 2011). The first step in the biosynthesis of camalexin is shared with that of Trp-derived glucosinolates and involves the conversion of Trp to its aldoxime by CYP79B2 or its homolog CYP79B3 (Glawischnig et al., 2004). The camalexin pathway then branches off with the action of CYP71A13, which converts the aldoxime to a nitrile (indole-3-acetonitrile [IAN]) (Nafisi et al., 2007). After an unknown activation step, GSTF6 catalyzes the conjugation to GSH to give GS-IAN (Su et al., 2011). Following the conjugation step, GS-IAN is hydrolyzed to Cys-IAN in a process in which the γ-glutamyl transpeptidases GGT1 and GGT2 and the phytochelatin synthase PCS1 have been proposed to be involved (Su et al., 2011). Finally, the multifunctional CYP71B15 catalyzes both the cyclization of Cys-IAN to give dihydrocamalexic acid (Schuhegger et al., 2006) and the oxidative decarboxylation of dihydrocamalexic acid to give camalexin (Böttcher et al., 2009).

This work provides evidence of the involvement of GSH as sulfur donor in the biosynthesis of glucosinolates by showing that an *Arabidopsis* double *ggp* mutant has altered glucosinolate levels and accumulates up to 10 related GSH conjugates. In addition, we demonstrate that GGPs serve a similar function in the biosynthesis of camalexin, since the *ggp* mutants are impaired in the production of camalexin and accumulate high amounts of the corresponding GSH conjugate GS-IAN. The involvement in the glucosinolate and camalexin pathways is supported by enzymatic assays and studies on cellular and subcellular localization.

RESULTS

The *Arabidopsis GGP* Gene Family

GGP1 has four homologous genes in *Arabidopsis*. Two of them, which we have named *GGP2* and *GGP3*, are arranged in tandem with *GGP1* on chromosome IV. The other two, which we have named *GGP4* and *GGP5*, are arranged in tandem on chromosome

II (see Supplemental Figure 1 online). Sequence analysis revealed that the encoded GGP proteins have amino acid identities ranging from 61 to 76% (see Supplemental Table 1 online). Analysis of public microarray-based expression data using Genevestigator (https://www.genevestigator.com/) showed that *GGP1* and *GGP3* exhibited high expression levels across all tissues. By contrast, the expression of *GGP4* was very low and confined to root tissues, and the expression of *GGP5* seemed to be restricted to pollen. Finally, *GGP2* seemed not to be expressed at all (see Supplemental Figure 2 online). Coexpression analyses using ATTED-II (http://atted.jp) showed that *GGP1* was the only *GGP* gene that was coregulated with known glucosinolate-related genes throughout all the available tissues.

Analysis of *ggp1* Mutants

The following publicly available *Arabidopsis* T-DNA mutants were analyzed by PCR for insertions in the *GGP1* gene: SALK_02930, SAIL_225_G01, GK-960B11, and GK-319F10. For the SALK and the SAIL lines, the T-DNA insertion could not be confirmed. From the two remaining lines, both with confirmed insertions in the first intron, only line GK-319F10 lacked the *GGP1* transcript in the homozygous state as seen by RT-PCR. We named this line *ggp1-1*. Relative transcript quantification by quantitative RT-PCR revealed that the homozygous *ggp1-1* mutant retained 0.7 to 1.0% of wild-type *GGP1* transcript levels.

We searched for a glucosinolate phenotype in leaves of the *ggp1-1* homozygous knockdown, but the levels of the different glucosinolates were unaltered in 3-week-old rosette leaves (data not shown). Based on publicly available microarray data, *GGP1* was the only *GGP* gene that was coregulated with known glucosinolate genes; however, the *GGP3* gene was also expressed throughout all tissues (see previous section and Supplemental Figure 2 online). We therefore hypothesized that the *GGP3* gene was able to substitute for the impaired *GGP1* function in the *ggp1-1* knockdown mutant. This would require three conditions to be met simultaneously: first, both genes should have overlapping expression patterns; second, both proteins must localize to the same subcellular compartment; and third, both proteins must catalyze the same enzymatic reactions.
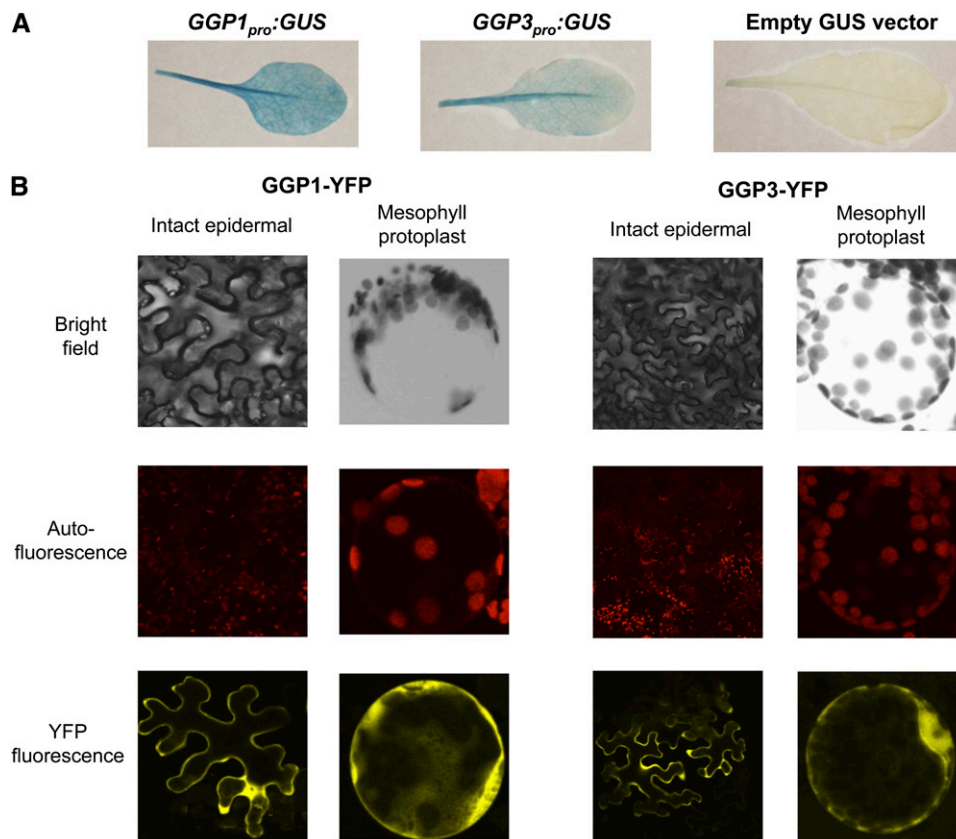

Figure 1. Cellular and Subcellular Localization of GGP1 and GGP3.

(A) GUS staining of rosette leaves of representative transgenic lines transformed with *GGP1*$_{pro}$:*GUS*, *GGP3*$_{pro}$:*GUS*, or empty vector as negative control. *GGP1*$_{pro}$:*GUS* plants were stained for 3 h, whereas *GGP3*$_{pro}$:*GUS* and control plants were stained for 6 h.
(B) CLSM analysis of intact epidermal cells and mesophyll protoplasts of *N. benthamiana* leaves transiently transformed with constructs coding for GGP1-YFP or GGP3-YFP (C-terminal fusions). Pictures were taken 7 d after infiltration with *Agrobacterium*.

Comparison of *GGP1* and *GGP3* Expression, Subcellular Localization, and Activity

The 2-kb promoter regions of *GGP1* and *GGP3* (*GGP1*$_{pro}$ or *GGP3*$_{pro}$, respectively) were cloned upstream of an open reading frame encoding β-glucuronidase (GUS). Along with an empty vector control, the resulting constructs were introduced separately into wild-type *Arabidopsis* Columbia-0 (Col-0) using *Agrobacterium tumefaciens*–mediated transformation. Leaf GUS analysis of at least three different lines per construct showed that both promoters conferred expression to (or in the vicinity of) vascular tissue (Figure 1A). The subcellular localization of GGP1 and GGP3 was investigated using C-terminal yellow fluorescent protein (YFP) fusions transiently expressed in leaves of *N. benthamiana* using *Agrobacterium*. The YFP fluorescence was visualized 7 d after infiltration using confocal laser scanning microscopy (CLSM), which showed that both protein fusions were cytosolic (Figure 1B).

We previously reported that GGP1 is able to enhance the production of BGLS in *N. benthamiana* by metabolizing the GSH conjugate that accumulates in its absence (GS-B) (Geu-Flores
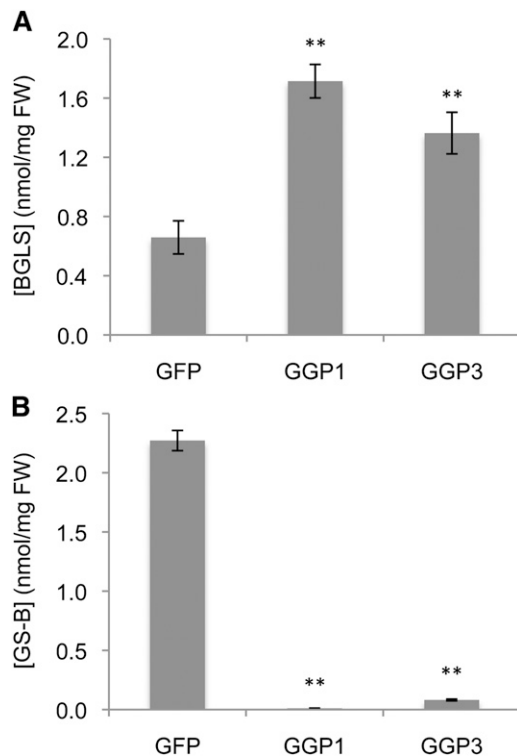
Table 1. Quantification of *GGP1* and *GGP3* Transcripts by Real-Time RT-PCR in Leaves of *ggp* Mutants Relative to Levels in Wild-Type Plants

Genotype	*GGP1* Transcript	*GGP3* Transcript
ggp1-1	0.7–1.0%	Unaltered
ggp3-1	Unaltered	3–13%
ggp1-1 ggp3-1	1–4%	6–30%

et al., 2009). We investigated whether GGP3 had the same effect as GGP1 in this heterologous system. The *APK2* gene was included in these experiments, as we have recently found that it ensures complete conversion of desulfoBGLS (the last intermediate in the pathway) to BGLS by satisfying the increased demand for activated sulfate (Møldrup et al., 2011). The experiments showed that GGP3 was able to enhance the accumulation of BGLS and suppress the accumulation of GS-B to almost the same extent as GGP1 (1.9-fold mean increase in BGLS compared with 2.4-fold for GGP1; 96.4% mean decrease in GS-B compared with 99.5% for GGP1) (Figure 2).

Downregulation of *GGP3* Using Artificial MicroRNAs and Construction of Double Knockdown Mutants

Since *GGP1* and *GGP3* are located ~2.5 kb apart on chromosome IV, the construction of a double T-DNA insertion mutant was not practically feasible. Instead, we decided to downregulate *GGP3* using artificial microRNA (amiRNA) (Ossowski et al., 2008) and to cross the resulting plants to the *ggp1-1* mutant. We made use of the Web MicroRNA Designer (http://wmd3.weigelworld.org/) for the design of two amiRNA constructs targeting *GGP3* and we assembled them using the USER fusion strategy (Nour-Eldin et al., 2010). The constructs were introduced separately into wild-type *Arabidopsis* Col-0 by *Agrobacterium*-mediated transformation. Using agarose gel-based RT-PCR, we screened all T1 transformants and selected the line with the lowest apparent *GGP3* transcript level. We called this line *ggp3-1*.

We then crossed the T1 *ggp3-1* amiRNA plant to a homozygous *ggp1-1* plant and used PCR to select F1 plants with both the amiRNA construct and the T-DNA insertion in the *GGP1* gene. Using a combination of PCR and segregation analysis, we generated comparable batches of T3 seeds coming from homozygous plants of each of the four following four genotypes: the wild type, *ggp1-1*, *ggp3-1*, and *ggp1-1 ggp3-1*. Comparative transcript analysis by real-time RT-PCR (quantitative RT-PCR) showed that the amiRNA construct was specific for *GGP3* and remained functional throughout several generations. Accordingly, transcript levels of both *GGP1* and *GGP3* were reduced in leaves of *ggp1-1 ggp3-1* plants and represented ~2 and ~18% of wild-type levels, respectively (Table 1).

ggp1-1 ggp3-1 Plants Have Altered GLS Levels and Accumulate Substantial Amounts of Glucosinolate-Related GSH Conjugates

Analysis of 3-week-old rosette leaves revealed a perturbed glucosinolate profile of *ggp1-1 ggp3-1* compared with wild-type

Figure 2. GGP-Aided Production of BGLS in *N. benthamiana*.

Leaves of *N. benthamiana* were infiltrated with a mixture of *Agrobacterium* strains carrying constructs that coded for P19 (silencing suppressor), CYP79A2, CYP83B1, SUR1, UGT74B1, SOT16, APK2, and GGP1, GGP3, or GFP (negative control). Each data point represents the mean of six biological replicates with error bars representing SE. Double asterisks indicate data points with highly significant differences compared with the GFP controls (P < 0.01 in unpaired Student's *t* tests).
(A) Accumulation of BGLS.
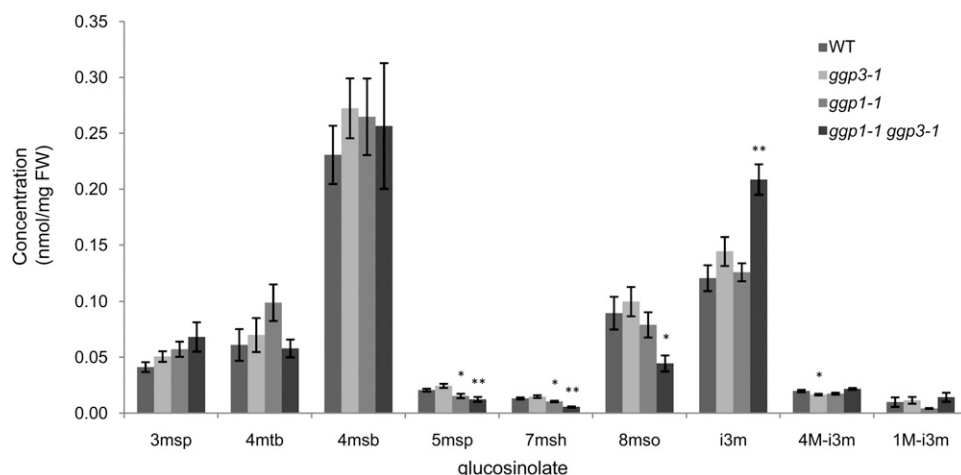**(B)** Accumulation of GS-B.
FW, fresh weight.

Figure 3. Glucosinolate Analysis of 3-Week-Old Rosette Leaves of Wild-Type, *ggp1-1*, *ggp3-1*, and *ggp1-1 ggp3-1* Plants.

Each data point represents the mean of eight biological replicates with error bars representing SE. Single and double asterisks indicate data points with significant or highly significant differences compared with their corresponding wild-type (WT) control (P < 0.05 or P < 0.01 in unpaired Student's *t* tests, respectively). 3msp, 3-(methylsulfinyl)propylglucosinolate; 4mtb, 4-(methylthio)butylglucosinolate; 4msb, 4-(methylsulfinyl)butylglucosinolate; 5msp, 5-(methylsulfinyl)pentylglucosinolate; 7msh, 7-(methylsulfinyl)heptylglucosinolate; 8mso, 8-(methylsulfinyl)octylglucosinolate; i3m, indole-3-yl-methylglucosinolate; 4M-i3m, 4-methoxyindole-3-yl-methylglucosinolate; 1M-i3m, 1-methoxyindole-3-yl-methylglucosinolate. FW, fresh weight.

plants (Figure 3, see legend for glucosinolate abbreviations). Whereas the levels of short-chained Met-derived glucosinolates (3msp, 4msb, and 4mtb) were not significantly altered, the levels of the long-chained ones were considerably reduced (5msp, 60% left; 7msh, 43% left; and 8mso, 50% left). Regarding Trp-derived glucosinolates, the levels of the most abundant one were increased (i3m, 1.7-fold higher) and the levels of its methoxylated

derivatives were unchanged (1M-i3m and 4M-i3m) (Figure 3). Induction experiments using methyl jasmonate did not result in further significant reduction of glucosinolate accumulation in induced *ggp1-1 ggp3-1* plants compared with induced wild-type controls (see Supplemental Figure 3 online). Although the fold induction for several glucosinolates appeared to be lower for *ggp1-1 ggp3-1* plants than for wild-type plants, these differences
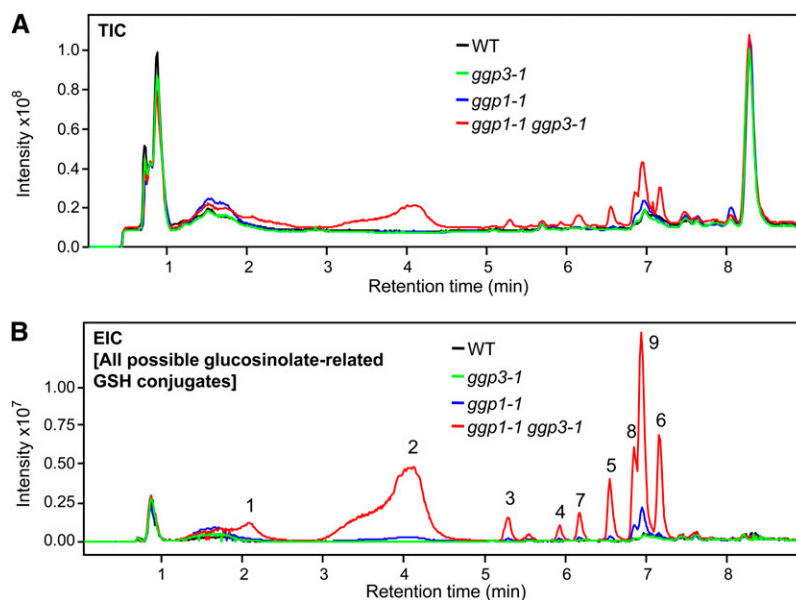

Figure 4. LC-MS Analysis of 3-Week-Old Rosette Leaves of Wild-Type, *ggp1-1*, *ggp3-1*, and *ggp1-1 ggp3-1* Plants.

(A) TICs. WT, wild type.
(B) EICs using the *m/z* ([M+H]$^+$) of all possible glucosinolate-related GSH conjugates. The identity of peaks 1 to 9 is specified in Table 2.

Table 2. Accurate Mass Measurements of the GSH Conjugates Found in Leaves of *ggp1-1 ggp3-1* Plants

Compound ID No.	Side Chain	Elemental Composition	Protonated Molecular Ion [M+H]$^+$		
			Theoretical *m/z*	Measured *m/z*	Error (ppm)
1	-(CH$_2$)$_3$(S=O)CH$_3$	C$_{15}$H$_{26}$N$_4$O$_8$S$_2$	455.1265	455.1257	−1.7
2	-(CH$_2$)$_4$(S=O)CH$_3$	C$_{16}$H$_{28}$N$_4$O$_8$S$_2$	469.1421	469.1425	+0.8
3	-(CH$_2$)$_5$(S=O)CH$_3$	C$_{17}$H$_{30}$N$_4$O$_8$S$_2$	483.1578	483.1587	+1.9
4	-(CH$_2$)$_6$(S=O)CH$_3$	C$_{18}$H$_{32}$N$_4$O$_8$S$_2$	497.1734	497.1744	+2.0
5	-(CH$_2$)$_7$(S=O)CH$_3$	C$_{19}$H$_{34}$N$_4$O$_8$S$_2$	511.1891	511.1898	+1.4
6	-(CH$_2$)$_8$(S=O)CH$_3$	C$_{20}$H$_{36}$N$_4$O$_8$S$_2$	525.2047	525.2052	+0.9
7	-(CH$_2$)$_3$SCH$_3$	C$_{15}$H$_{26}$N$_4$O$_7$S$_2$	439.1316	439.1318	+0.5
8	-(CH$_2$)$_4$SCH$_3$	C$_{16}$H$_{28}$N$_4$O$_7$S$_2$	453.1472	453.1474	+0.4
9	Indol-3-ylmethyl-	C$_{20}$H$_{26}$N$_5$O$_7$S	480.1548	480.1540	−1.6

were not significant in two-way analysis of variance tests (e.g., P = 0.053 for i3m) (see Supplemental Figure 3 online).

To investigate the accumulation of intermediates in leaves of the single and double mutants, we performed an untargeted metabolite analysis by liquid chromatography–mass spectrometry (LC-MS). As seen in total ion chromatograms (TICs), the metabolite profile of leaf extracts did not vary visibly in the single *ggp1-1* and *ggp3-1* mutants when compared with the wild type. However, the profile of the *ggp1-1 ggp3-1* leaves was dramatically different because of the appearance of several abundant peaks (Figure 4A). Inspection of the mass spectrum of these peaks showed that all of them corresponded to GSH conjugates that could potentially be intermediates in the biosynthesis of glucosinolates. Extracted ion chromatograms (EICs) using the masses of all theoretically possible glucosinolate-related GSH conjugates showed that *ggp1-1 ggp3-1* plants accumulated nine different GSH conjugates (Figure 4B; Table 2) and that most, if not all, of the variation seen in the TICs was due to these accumulating compounds. The EICs also showed that the *ggp1-1* mutant accumulated traces of these compounds, whereas the *ggp3-1* mutant and the wild type did not accumulate them at all. The identity of the GSH conjugates was confirmed by accurate mass determination (Table 2) and fragmentation analysis (see Supplemental Table 2 online).

The *ggp* Mutants Produce Less Camalexin and Accumulate the Related GSH Conjugate upon Induction

We investigated whether the *ggp* mutants had a camalexin phenotype by inducing camalexin production in 3-week-old rosette leaves with AgNO$_3$ and analyzing leaf extracts 24 h later using HPLC coupled to a fluorescence detector. Whereas the *ggp3-1* mutant did not accumulate significantly less camalexin than the wild type, the *ggp1-3* mutant accumulated ∼40%, and the *ggp1-1 ggp3-1* double mutant accumulated ∼11% of wild-type camalexin levels (Figure 5A).

We used LC-MS to search for the GSH conjugate of the camalexin intermediate IAN (GS-IAN) in the same leaf extracts. Whereas both the wild type and the *ggp3-1* mutant accumulated trace amounts of a compound with the mass of GS-IAN, both *ggp1-1* and the double *ggp1-1 ggp3-1* mutant accumulated very high amounts of this compound. We confirmed that this compound was GS-IAN by chemically synthesizing a standard and

comparing retention times and fragmentation patterns (Figures 5B and 5C). Quantification of GS-IAN in the leaf extracts showed that the *ggp1-1* mutant and the *ggp1-1 ggp3-1* double mutant produced a similar amount of GS-IAN (200 to 300 pmol/mg fresh weight), which was comparable to the amount of camalexin produced by wild-type plants (Figure 5D).

Recombinant GGP1 and GGP3 Can Metabolize Glucosinolate-Related GSH Conjugates and GS-IAN

As final proof of the multiple and overlapping enzymatic activities of GGP1 and GGP3, we expressed their His-tagged versions in *Escherichia coli* and analyzed the activity of the purified proteins in vitro. As substrates, we used either synthetic GS-IAN (camalexin intermediate) or extracts of *ggp1-1 ggp3-1* leaves containing the different glucosinolate-related conjugates. In the extracts, an additional glucosinolate-related conjugate was detected, which had a side chain corresponding to the glucosinolate 5mtp (compound ID# 10; accurate mass error of +1.6 ppm compared with theoretical mass; see Supplemental Table 2 online). The assays with the extracts showed that both GGP1 and GGP3 were able to metabolize nine out of 10 GSH conjugates to the corresponding enzymatic products (Cys-Gly conjugates), all of which spontaneously rearranged to their cyclized forms as previously seen for GS-B (Geu-Flores et al., 2009). The cyclized Cys-Gly conjugates were readily detectable in GGP1 and GGP3 reaction mixtures and virtually absent in control mixtures, where only trace amounts near detection limits were observed (Figure 6). A notorious exception was the cyclized Cys-Gly conjugate related to the glucosinolate 4msb, which was also present in control mixtures (Figure 6). The identity of all detectable cyclized Cys-Gly conjugates was confirmed by accurate mass determination (Table 3) and fragmentation analysis (see Supplemental Table 3 online). Finally, the assays with GS-IAN showed that both GGP1 and GGP3 were able to yield a compound with mass and fragmentation patterns consistent with the Cys-Gly conjugate of IAN (Cys-Gly-IAN) (Figure 7).

DISCUSSION

This article provides direct genetic evidence of the involvement of GSH as sulfur donor in the biosynthesis of glucosinolates. The
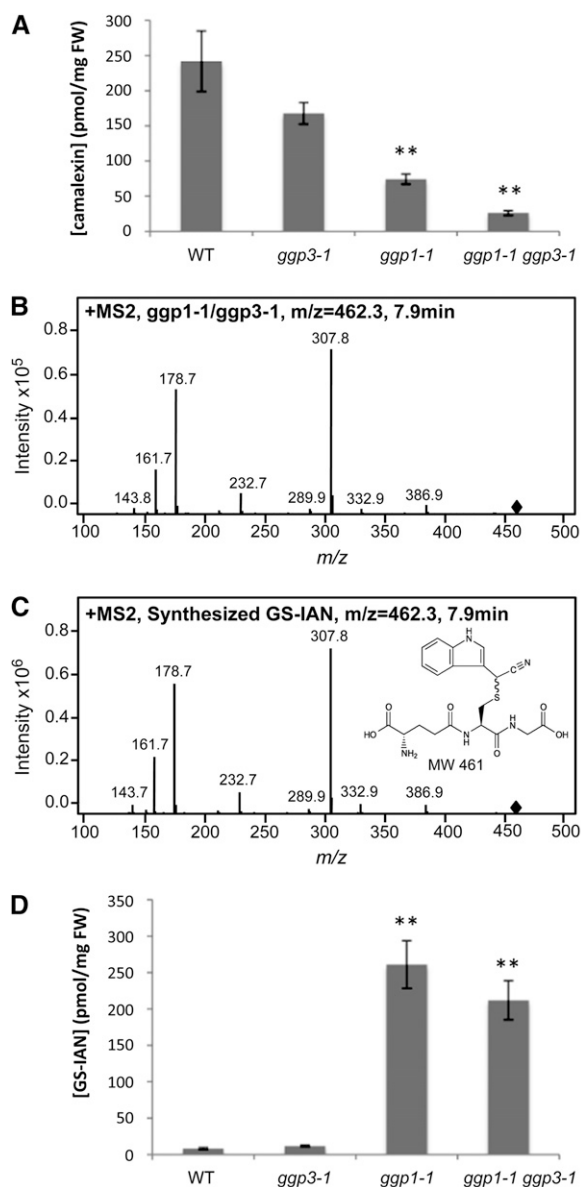
Figure 5. Metabolite Analysis of 3-Week-Old Rosette Leaves of Wild-Type, *ggp1-1*, *ggp3-1*, and *ggp1-1 ggp3-1* Plants 24 h after Induction with AgNO₃.

(A) Quantification of camalexin by HPLC-fluorescence in the different genotypes. FW, fresh weight; WT, wild type.

(B) MS2 fragmentation of the m/z = 462.3 ion highly abundant in the LC-MS analysis of *ggp1-1* and *ggp1-1 ggp3-1* mutants. The diamond indicates the mass of the mentioned ion.

(C) MS2 fragmentation of the m/z = 462.3 ion from the LC-MS analysis of synthetic GS-IAN. The diamond indicates the mass of the mentioned ion.

(D) Quantification of GS-IAN by LC-MS in the different genotypes. Each data point represents the mean of eight biological replicates with error bars representing SE. Double asterisks indicate data points with highly significant differences compared with the wild type (P < 0.01 in unpaired Student's *t* tests).

evidence surfaced from the analysis of *Arabidopsis* mutants impaired in the production of GGPs. Specifically, the *ggp1-1 ggp3-1* double knockdown mutant showed an altered foliar glucosinolate profile and accumulated up to 10 different GSH conjugates related to glucosinolate biosynthesis. Our data on cellular and subcellular localization of GGP1 and GGP3 are consistent with a glucosinolate biosynthetic role. Indeed, published promotor-GUS fusion experiments performed with core glucosinolate biosynthetic genes have all shown a similar expression in leaf vascular tissues (Mikkelsen et al., 2000; Reintanz et al., 2001; Tantikanjana et al., 2001, 2004; Chen et al., 2003; Grubb et al., 2004; Kusnierczyk et al., 2007). Furthermore, the cytosolic localization of the GGP1- and GGP3-GFP (green fluorescent protein) fusions is in agreement with the proposed cytosolic localization of the core glucosinolate pathway. The latter is based on the association of cytochromes P450 with the endoplasmic reticulum, with their catalytic domain facing the cytosol (relevant for CYP79s and CYP83s) (Schuler and Werck-Reichhart, 2003), and on the lack of predicted targeting peptides of the known soluble enzymes (SUR1, UGT74B1, and SOT16, 17, and 18), experimentally shown for the SOTs (Klein et al., 2006). Combined with biochemical in vitro data showing the ability of both GGPs to use at least nine out of 10 of the accumulating GSH conjugates as a substrates, we conclude that GGP1 and GGP3 are enzymes metabolizing GSH conjugates in the glucosinolate pathway in *Arabidopsis*. In accordance with this, we conclude that the reduced sulfur atom in the core glucosinolate structure is derived from GSH.

The fact that the levels of only long-chained Met-derived glucosinolates were reduced in *ggp1-1 ggp3-1* plants (and not the levels of all glucosinolates) may reflect that the mutant was a double knockdown mutant and not a double knockout mutant. In other words, the residual *GGP1* and *GGP3* transcripts (up to 4 and 30% of wild-type levels, respectively) are likely to have generated sufficient protein so as to prevent a more marked phenotype. Furthermore, the increase in levels of the main Trp-derived glucosinolate (i3m) in *ggp1-1 ggp3-1* resembles a similar increase in i3m observed in another mutant deficient in Met-derived glucosinolates, namely, *cyp83a1* (Hemm et al., 2003). This provides additional evidence of a complex interplay between the productions of Met- and Trp-derived glucosinolates in *Arabidopsis*. Regardless of the subtle glucosinolate end-product phenotype, the *ggp1-1 ggp3-1* double mutant accumulated substantial amounts of GSH conjugates not only related to the glucosinolates with decreased levels, but also related to all other glucosinolates normally present in wild-type leaves (Kliebenstein et al., 2001).

The accumulation of GSH conjugates with sulfinyl side chains (compounds 1 to 6) is unexpected as side chain modifications such as the oxidation of thio to sulfinyl glucosinolates (e.g., the oxidation of 4-mtb to 4-msb) are believed to happen after the GGP step. However, it was shown for FMO_GS-OX1 (catalyzing the mentioned oxidation) that the reaction can occur not only at the glucosinolate level, but also at the desulfoglucosinolate level (Hansen et al., 2007). A possible explanation could be that FMOs can also act at the GSH conjugate level, converting the accumulating thio GSH conjugates to sulfinyl GSH conjugates. An alternative explanation could be that the thio and sulfinyl side
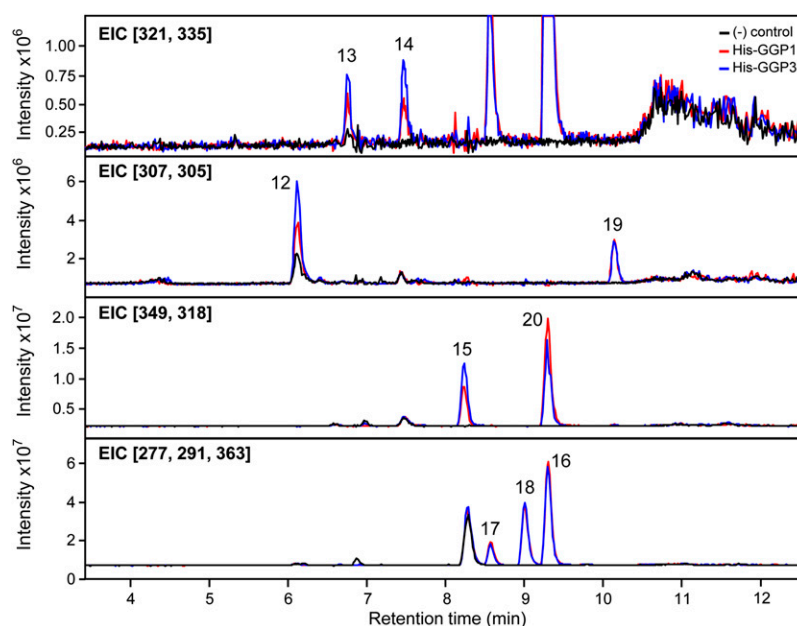
Figure 6. LC-MS Analysis of Enzymatic Assays Using His-Tagged GGP1 or GGP3 with an Extract from *ggp1-1 ggp3-1* Plants.

Protein from an expression strain carrying the empty vector was used as negative control. Four different EICs (extracted masses) accounting for nine cyclized Cys-Gly conjugates are presented. The identity of each marked peak is specified in Table 3.

chains are subject to nonenzymatic interconversions dependent on redox levels of the surrounding medium. Either proposition could explain not only the accumulation of compounds 1 to 6, but also the absence of the thio GSH conjugates related to 7-mtp and 8-mto, whose sulfinyl counterparts were abundant in the double mutant (compounds 5 and 6). The accumulation of cyclized Cys-Gly conjugate related to the glucosinolate 4-msb (Figure 6, compound 12) is also worth discussing, since the mentioned compound accumulated in *ggp1-1 ggp3-1* mutants, but not in wild-type plants (see Supplemental Figure 4 online). Considering that 4-msb is the most abundant glucosinolate in *Arabidopsis* leaves, a possible explanation is that the related

GSH conjugate (compound 2) accumulated to such extent that it entered the default xenobiotic detoxification pathway. As mentioned in the Introduction, GSH conjugates of xenobiotics are transported to the vacuole, where they are initially cleaved by a GGT. Vacuolar cleavage of compound 2 in the absence of the rest of the glucosinolate biosynthetic machinery could lead to cyclization and, thus, to a metabolic dead end.

Our results also demonstrate that GGPs are involved in camalexin biosynthesis, since leaves of the single *ggp1-1* mutant were impaired in the accumulation of the phytoalexin when compared with wild-type leaves, and the double mutant *ggp1-1 ggp3-1* accumulated even less camalexin. In addition, both of

Table 3. Accurate Mass Measurements of the Cyclized Cys-Gly Conjugates Found in Enzymatic Assays Using Extracts of *ggp1-1 ggp3-1* Leaves and Recombinant GGP1 or GGP3

			Protonated Molecular Ion [M+H]⁺		
Compound ID No.	Side Chain	Elemental Composition	Theoretical *m/z*	Measured *m/z*	Error (ppm)
11	-(CH$_2$)$_3$(S=O)CH$_3$	C$_{10}$H$_{16}$N$_2$O$_4$S$_2$	293.0624	n.d.	n.d.
12	-(CH$_2$)$_4$(S=O)CH$_3$	C$_{11}$H$_{18}$N$_2$O$_4$S$_2$	307.0781	307.0777	−1.2
13	-(CH$_2$)$_5$(S=O)CH$_3$	C$_{12}$H$_{20}$N$_2$O$_4$S$_2$	321.0937	321.0921	−5.0
14	-(CH$_2$)$_6$(S=O)CH$_3$	C$_{13}$H$_{22}$N$_2$O$_4$S$_2$	335.1094	335.1095	+0.4
15	-(CH$_2$)$_7$(S=O)CH$_3$	C$_{14}$H$_{24}$N$_2$O$_4$S$_2$	349.1250	349.1246	−1.2
16	-(CH$_2$)$_8$(S=O)CH$_3$	C$_{15}$H$_{26}$N$_2$O$_4$S$_2$	363.1407	363.1408	+0.3
17	-(CH$_2$)$_3$SCH$_3$	C$_{10}$H$_{16}$N$_2$O$_3$S$_2$	277.0675	277.0681	+2.1
18	-(CH$_2$)$_4$SCH$_3$	C$_{11}$H$_{18}$N$_2$O$_3$S$_2$	291.0832	291.0839	+2.5
19	-(CH$_2$)$_5$SCH$_3$	C$_{12}$H$_{20}$N$_2$O$_3$S$_2$	305.0988	305.0985	−1.0
20	Indol-3-ylmethyl-	C$_{15}$H$_{15}$N$_3$O$_3$S	318.0907	318.0908	+0.3

n.d., not determined.

these mutants accumulated high amounts of the related GSH conjugate GS-IAN. Our results on the cytosolic localization of GGP1 and GGP3 are consistent with the likely cytosolic localization of the camalexin pathway. Indeed, three of the four known enzymes in the pathway (including the first and the last one) are cytochromes P450, which are associated with the endoplasmic reticulum, having their catalytic domain facing the cytosol (Schuler and Werck-Reichhart, 2003). The fourth enzyme, GSTF6, lacks predicted signaling peptides and is therefore most likely cytosolic. In combination with the in vitro biochemical evidence showing that both GGPs were able to use synthetic GS-IAN as a substrate, we conclude that GGP1 and GGP3 are enzymes metabolizing GS-IAN in the camalexin pathway.
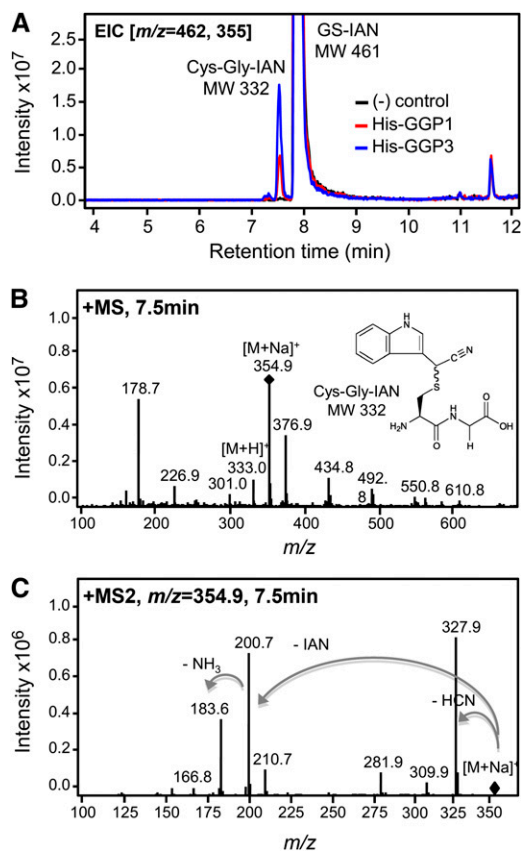

Figure 7. LC-MS Analysis of Enzymatic Assays Using His-Tagged GGP1 or GGP3 with GS-IAN as Substrate.

Protein from an expression strain carrying the empty vector was used as negative control.

(A) EICs using masses corresponding to the substrate ([M+H]+ of 462) and the product ([M+Na]+ of 355).

(B) MS spectrum of the product peak at 7.5 min. The structure of the product, Cys-Gly-IAN, is shown.

(C) MS2 fragmentation of the m/z = 354.9 ion corresponding to the [M+Na]+ adduct of Cys-Gly-IAN. The diamond indicates the mass of the mentioned ion. The arrows represent possible relations between parent and daughter ions.
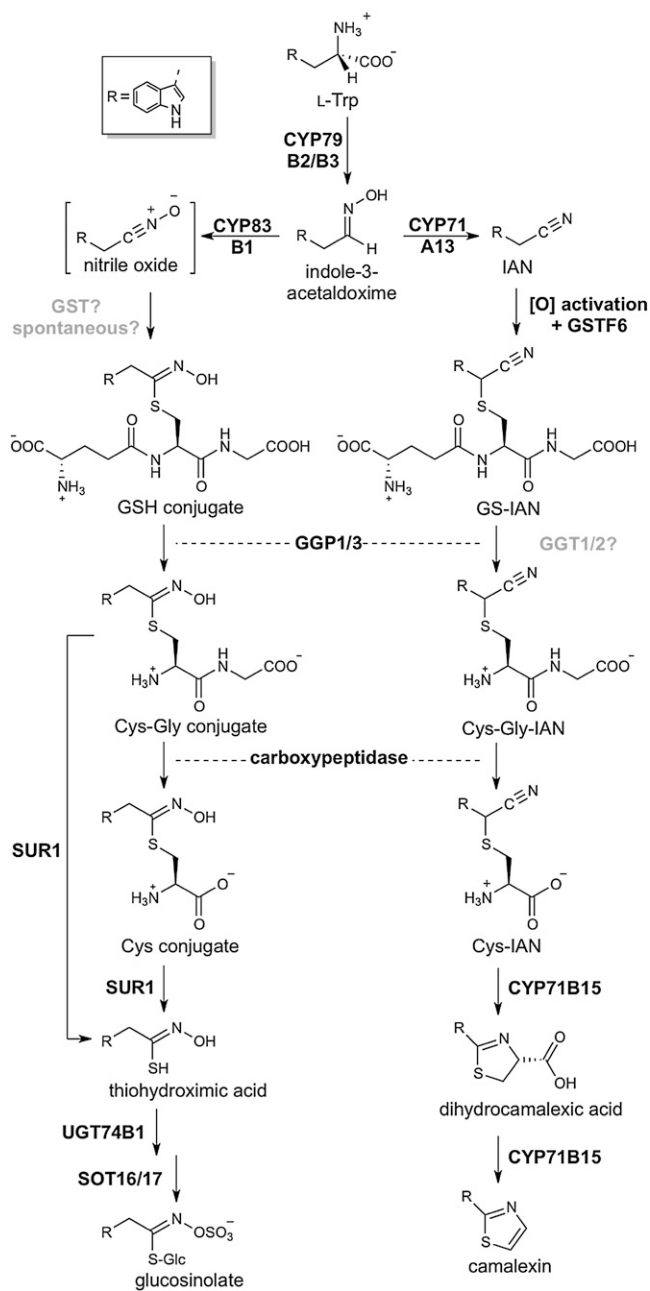

Figure 8. Proposed Model for the Biosynthesis of Trp-Derived Glucosinolates and Camalexin in *Arabidopsis*.

The pathway leading to Trp-derived glucosinolates is represented in the left branch, and the pathway leading to camalexin is represented in the right branch. As indicated in the boxed insert, R represents an indole-3-yl group. Since it is not currently known whether the substrates of SUR1 are the Cys-Gly conjugates or the Cys conjugates (see Discussion), both possibilities have been depicted.

GGP1 and GGP3 are the only known plant enzymes capable of hydrolyzing the γ-glutamyl residue of GSH conjugates in the cytosol, since the only other enzymes with similar activities, the GGTs, are located either in the extracellular space (GGT1 and GGT2) (Martin et al., 2007; Ohkama-Ohtsu et al., 2007a) or in the vacuole (GGT4) (Grzam et al., 2006; Ohkama-Ohtsu et al., 2007b). Indirect evidence for cytosolic γ-glutamyl peptidase activity was presented by Grzam et al. (2006), who showed that the vacuolar sequestration of GS-bimane in wild-type *Arabidopsis* leaves could be efficiently inhibited by azide (N_3^-); however, its degradation to the Cys conjugate proceeded normally, perhaps even at a faster rate. This observation pointed to the presence of an efficient cytosolic γ-glutamyl peptidase and can now possibly be explained by the existence of GGP1 and GGP3.

Recently, Su et al. (2011) suggested a role for GGT1 and GGT2 in the processing of GS-IAN in camalexin biosynthesis. Their suggestion is based on the lower camalexin content of *ggt1* and *ggt2* mutants when compared with a wild-type plant and on the lower camalexin content of wild-type plants when treated with the GGT inhibitor acivicin. The camalexin phenotype in the mutants is surprising given the proven extracellular localization of the GGTs (see above). The inhibition experiments cannot be taken as conclusive in favor of the involvement GGTs, since acivicin is likely to inhibit GGPs as well. Moreover, GGP1 and GSTF6 were found among the 20 proteins whose levels were increased upon MKK9-induced camalexin production, whereas GGT1 and GGT2 were not (Su et al., 2011). Future studies are needed to explain the interesting camalexin phenotype seen upon knockout of the extracellular GGTs, including the search for accumulating intermediates in the knockouts.

The glucosinolate and camalexin pathways have been suggested to have a biogenetic relationship (Rauhut and Glawischnig, 2009), and the involvement of GGPs in both pathways supports this hypothesis. In the camalexin pathway, another peptidase, a carboxypeptidase, is required to hydrolyze the Cys-Gly peptide bond to give the established intermediate Cys-IAN. Su et al. suggested PCS1 as a candidate; however, their own data showed that the *pcs1-1* mutant was not significantly reduced in camalexin accumulation upon biotic treatment in comparison to wild-type plants (Su et al., 2011). In the absence of further evidence, we consider the carboxypeptidase as unknown. This second peptidase may or may not be part of the glucosinolate pathway, as it is currently unknown whether the Cys-Gly conjugates or the Cys-conjugates are the substrates of the next known enzyme in the pathway, SUR1. Like any other *C-S* lyase, SUR1 requires its substrates to have a free amino group in the Cys moiety (Schwimmer and Kjaer, 1960), and both types of conjugates (but not GSH conjugates) fulfill this requirement. However, given the likely biogenetic relationship between the two pathways and the broader distribution of glucosinolates throughout the Brassicales order (Rauhut and Glawischnig, 2009), it is possible that the GGPs and the unknown carboxypeptidase were recruited together to the camalexin pathway from the glucosinolate pathway. Our current model for glucosinolate and camalexin biosynthesis in *Arabidopsis* is outlined in Figure 8.

Until the discovery of GGPs, GGTs were the only known plant enzymes capable of hydrolyzing GSH conjugates (Martin et al., 2007). It is noteworthy that GGPs are not related to GGTs but are

related to Gln amidotransferases, enzymes that transfer the amido nitrogen of Gln to different acceptor substrates (Mouilleron and Golinelli-Pimpaneau, 2007). Two other enzymes related to Gln amidotransferases have been linked to unexpected biochemical reactions. The first one is puuD from *E. coli*, which has been shown to catalyze the hydrolysis of γ-glutamyl-γ-aminobutyrate in the utilization pathway of putrescine (Kurihara et al., 2005, 2006). The second one is DUG3 from the yeast *Saccharomyces cerevisiae*, which has been linked to the hydrolysis of the γ-Glu-Cys peptide bond of GSH in a previously unknown GSH degradation pathway (Ganguli et al., 2007), although proof of its direct catalysis is missing. The structural resemblance between Gln, GSH conjugates, γ-glutamyl-γ-aminobutyrate, and GSH, namely, the shared γ-glutamyl moiety, provides an explanation for the unexpected activities of GGPs, puuD and DUG3, and suggest that only the γ-glutamyl moiety is crucial for substrate recognition. This is supported by the fact that both GGP1 and GGP3 are able to use nine different glucosinolate-related GSH conjugates and the camalexin-related GS-IAN as substrates. Further studies need to be performed to determine the extent of this partial promiscuity. Particularly interesting is whether GGP1 and GGP3 can hydrolyze GSH, since their ubiquitous expression and cytosolic localization (where GSH is abundant) suggest that they cannot.

In summary, our results demonstrate that GSH is the sulfur donor in the biosynthesis of glucosinolates and that GGP1 and GGP3 are cytosolic enzymes metabolizing GSH conjugates in the biosynthesis of both glucosinolates and camalexin in *Arabidopsis*.

METHODS

Plant Materials and Growth Conditions

Arabidopsis thaliana lines SALK_02930 and SAIL_225_G01 were obtained from the ABRC (Alonso et al., 2003). *Arabidopsis* lines GK-960B11 and GK-319F10 (renamed *ggp1-1*) were obtained from the University of Bielefeld (Bielefeld, Germany) (Rosso et al., 2003). All *Arabidopsis* plants were grown in growth chambers at 20°C and 70% relative humidity with 16-h photoperiods at $100 \, \mu E \, m^{-2} \, s^{-1}$. All *Nicotiana benthamiana* plants were grown in a greenhouse with a day/night regime of 28/25°C and 16-h-long days.

Identification of GGP Family Members and Sequence Analysis

The annotated amino acid sequence of GGP1 (NP_194782) was used as input in a position-specific iterated BLAST search using the Reference Protein database (refseq_protein) at the National Center for Biotechnology Information limited to *Arabidopsis* sequences. The search was terminated after the third iteration. Four homologs were identified. Sequence identities were determined by pairwise alignment using ClustalW (default settings).

Genotyping of Potential *ggp1* Mutants

Line SALK_02930 was genotyped using primers 5′-TTGAGCCATAGA-GGGAAAATG-3′ and 5′-TTGCCTTGCTGGTATAAACTTATG-3′, together with the SALK left-border primer 5′-TGGTTCACGTAGTGGGCCATCG-3′. Line SAIL_225_G01 was similarly genotyped using primers 5′-GGAAT-ACGCAAGCACTTTAG-3′, 5′-TTTTGTCATTTCAACTTTTAATTATTGG-3′, and the SAIL left-border primer 5′-ATTTTGCCGATTTCGGAAC-3′. Lines

GK-960B11 and GK-319F10 were both genotyped using primers 5′-AGA-TACGCTCTGTTTCTAGC-3′, 5′-GCTTAGGTTCTTCTTATTCA-3′, and the GK left-border primer 5′-ATATTGACCATCATACTCATTGC-3′.

Cellular Localization Using Promoter-GUS Fusions

The 2-kb promoter regions of *GGP1* and *GGP3* were amplified from wild-type (Col-0) *Arabidopsis* genomic DNA using primer pairs 5′-GGCTT-AAUGCACGTAGGCAATGACTTGTGAGGT-3′/5′-GGTTTAAUTTTTTTT-GTTCTGGCTAAATGAAAATACAAAGATTGATTG-3′ and 5′-GGCTTAAU-TGGCATATGCTTTGGTCACCAGG-3′/5′-GGTTTAAUCTTCTTCTTCTTT-CGTCTCAGAGATCACA-3′, respectively. The amplified promoters were USER cloned (Nour-Eldin et al., 2010) into pBGF-0u (Nour-Eldin et al., 2006), which provided a downstream open reading frame encoding a nuclear-localized GFP fused to GUS (nls-GFP-GUS) (Chytilova et al., 1999). Along with the empty vector, the constructs were transformed into wild-type (Col-0) *Arabidopsis* using *Agrobacterium tumefaciens*–mediated transformation (floral dip). Transformants were selected by spraying with Basta and genotyped using a mix of three primers, 5′-GTTTGTCTACAAATGATATCCATGTTC-3′, 5′-CCGGACACGCTGAA-CTTGT-3′, and 5′-GACAGCTAATCTCGATGTGTGATTCT-3′, which gave amplicons of different sizes for the two different insertions. At least three different lines per genotype were analyzed using conventional GUS assays (including ferri- and ferrocyanide) (Caissard et al., 1994) on detached 3-week-old rosette leaves.

Subcellular Localization Using YFP Fusions

The coding regions of GGP1 and GGP3 were amplified without stop codons from cDNA clones RAFL06-16-J02 (RIKEN BioResource Center) and U21128 (ABRC) using primer pairs 5′-GGCTTAAUATGGTGGAG-CAAAAGAGATACGC-3′/5′-GGTTTAAUCCGTTAGTTGGAACTCTGCCT-TTG-3′ and 5′-GGCTTAAUATGGTGGTTATTGAGCAGAAG-3′/5′-GGTT-TAAUCCACCTTTCAGGAAGTTTTTGCAG-3′, respectively. The amplified coding regions were USER-cloned (Nour-Eldin et al., 2010) into pPS48YFPu (Nour-Eldin et al., 2006), which provided a downstream YFP coding region (Venus version) (Nagai et al., 2002). The constructs were transformed into *Agrobacterium* and infiltrated into leaves of 3-week-old *N. benthamiana* plants as described by Voinnet et al. (2003). Seven days after infiltration, YFP fluorescence was visualized in intact epidermal cells and in mesophyll protoplasts by CLSM. Epidermal cells were examined directly on the surface of small leaf pieces, and mesophyll protoplasts were prepared using the Tape-*Arabidopsis* Sandwich method (Wu et al., 2009). CLSM was performed on a Leica TCS SP2/MP microscope. YFP was excited at 514 nm, and emissions were recorded in the interval 525 to 540 nm.

GGP Functionality Assay in *N. benthamiana*

The coding region of *GGP3* was amplified from the cDNA clone U21128 (ABRC) using primers 5′-GGCTTAAUATGGTGGTTATTGAGCAGAAG-3′ and 5′-GGTTTAAUTCAACCTTTCAGGAAGTTTTTG-3′ and USER cloned (Nour-Eldin et al., 2010) into pCAMBIA3300-35Su (Nour-Eldin et al., 2006). Transient coexpression with the BGLS-producing constructs ORF1 and ORF2 was achieved in leaves of *N. benthamiana* as described previously for GGP1 (Geu-Flores et al., 2009). Analysis of BGLS (desul-foglucosinolate method, HPLC-UV based) and of GS-B (LC-MS based) was performed as described previously (Geu-Flores et al., 2009).

Construction of amiRNA Lines Targeting *GGP3*

Two microRNA constructs targeting *GGP3* were designed using the Web MicroRNA Designer (http://wmd3.weigelworld.org/). The corresponding

plant transformation constructs were assembled into pCAMBIA3300-35Su using the USER fusion strategy (Ossowski et al., 2008; Nour-Eldin et al., 2010). All PCR fragments were amplified from pRS300 (Ossowski et al., 2008). The fragment carrying the microRNA loop was amplified using the primer pair 5′-AAAGAGAAUCAATGATCCAATTTGTCTAC-3′/5′-GGTTTAAUGTGGATCCCCCCCATGGCGATGC-3′ and was the same for both constructs. For construct 1, the flanking fragments were amplified using primer pairs 5′-ACGACCTGUGAATAGTAAATATCT-GGTGGTCGTCTACATATATATTCCTA-3′/5′-GGCTTAAUTCGAATTCC-TGCAGCCCCAAAC-3′ and 5′-ATTCTCTTUGATTAGTAATTATCT-GGTGGGCGTCTCTCTTTTGTATTCCA-3′/ 5′-GGTTTAAUGTGGATCC-CCCCATGGCGATGC-3′. For construct 2, primer pairs 5′-ACGAC-CTGUGAATTCATAATAAGGACTCGTTCTCTACATATATATTCCTA-3′/5′-GGCTTAAUTCGAATTCCTGCAGCCCCAAAC-3′ and 5′-ATTCTC-TTUGATTTCATATTAAGGACTCGCTCTCTCTCTTTTGTATTCCA-3′/5′-GGTTTAAUGTGGATCCCCCCCATGGCGATGC-3′ were used. The constructs were introduced into wild-type (Col-0) *Arabidopsis* by *Agrobacterium*-mediated transformation using the floral dip method. Transformants were selected by spraying with the herbicide Basta and by PCR using primers 5′-GGCTTAAUTCGAATTCCTGCAGCCC-CAAAC-3′ and 5′-GGTTTAAUGTGGATCCCCCCCATGGCGATGC-3′.

Construction of the *ggp1-1 ggp3-1* Double Mutant

The selected T1 *ggp3-1* amiRNA plant, which was derived from amiRNA construct 1, was crossed to homozygous *ggp1-1* plants, and F1 plants with both the amiRNA construct and the T-DNA insertion in the *GGP1* gene were selected by PCR as described for the parental lines. We then used multiplex PCR to select F2 plants that were either wild-type for the *GGP1* locus or *ggp1-1* homozygous, each selected plant either having or lacking the amiRNA construct. For the phenotypic analysis, F3 seed batches were obtained from each selected F2 plant. For the genotypes having the amiRNA construct, 40 seedlings from each seed batch were sprayed with the Basta to select batches where the amiRNA construct (linked to the Basta resistance gene) did not segregate out. Only the seed batches where no seedlings died were subjected to phenotypic analysis.

Transcript Analysis of *ggp* Mutant Plants

Total RNA was extracted from 3-week-old rosette leaves using the Nucleo-Spin RNA II kit (Macherey-Nagel), including on-column DNase treatment. RNA concentration was estimated spectrophotometrically (Nano Drop ND-1000; Thermo Scientific). cDNA was synthesized from 2 μg RNA using the iScript cDNA synthesis kit (Bio-Rad). Screening of T1 amiRNA transformants was performed by agarose gel-based RT-PCR. Amplification of *GGP1*, *GGP3*, and *Actin* (At3g18780) fragments was performed using the intron-spanning primer pairs 5′-TCACGATGCCTTTGAGAATGAT-3′/5′-AACTTCCAGGCGTAATC-GCA-3′, 5′-TGATGCTTTCGGGAGACGCC-3′/5′-AAAGTAACCTCGTAGTTTT-TCATTG-3′, and 5′-ACATTGTGCTCAGTGGTGGA-3′/5′-TCATACTCGGCC-TTGGAGA-3′, respectively.

For the quantification of *GGP1* and *GGP3* transcripts in the single and double mutants, real-time RT-PCR (quantitative PCR) was performed using a Rotor-Gene 6000 (Corbett Life Science/Qiagen) and the DyNAmo Flash SYBR Green qPCR kit (Finnzymes) in total reaction volumes of 20 μL. The primers used were the same as specified for the screening of T1 amiRNA transformants. For all primer pairs, efficiency and linear ampli-fication ranges were determined. For each genotype, three biological replicates were used, each measured in triplicate.

Routine Metabolite Analyses of *ggp* Mutant Plants

All metabolite analyses were performed using rosette leaves of 3-week-old plants. Glucosinolate analysis was performed using the

desulfoglucosinolate method (HPLC-UV based) as described by Hansen et al. (2007), except that fresh leaves were harvested into methanol and subsequently crushed. For induction experiments, whole plants were sprayed with either 250 μM methyl jasmonate in 0.25% ethanol or with 0.25% ethanol (mock solution) 24 h prior to harvesting. The glucosinolate sinigrin (not present in *Arabidopsis*) was used as an internal standard together with published response factors for the individual glucosinolates (Brown et al., 2003). Untargeted analysis by LC-MS was performed on a fraction of the spun-down methanolic extracts as previously described (Geu-Flores et al., 2009).

For the analysis of camalexin, nondetached leaves were induced by covering the adaxial side with small droplets of 5 mM AgNO$_3$. The induction procedure was repeated 12 h later. Twenty-four hours after the initial induction, entire leaves were harvested and crushed in methanol. After spinning down twice, camalexin analysis by HPLC fluorescence was performed as described by Schuhegger et al. (2006). Quantification was achieved using synthetic camalexin as external standard, kindly provided by David P. Dixon (Durham University, Durham, UK). A fraction of the spun-down methanolic extracts was analyzed by LC-MS as previously described (Geu-Flores et al., 2009). The accumulated GS-IAN was quantified using synthetic GS-IAN as external standard.

Accurate Mass Determination and Fragmentation Analysis

Chromatographic separations were performed on an Acquity UPLC system (Waters) equipped with a HSS T3 column (100 × 1.0 mm, particle size 1.8 μm; Waters) applying the following binary gradient at a flow rate of 150 μL min^{-1}: 0 to 1 min, isocratic 95% A (water, 0.1% formic acid), 5% B (acetonitrile, 0.1% formic acid); 1 to 6 min, linear from 5 to 30% B; 6 to 10 min, linear from 30 to 95% B; 10 to 12 min, isocratic 95% B; 12 to 14 min, isocratic 5% B. Eluted compounds were detected from mass-to-charge ratio (*m/z*) 100 to 1000 using a MicrOTOF-Q II hybrid quadrupole time-of-flight mass spectrometer (Bruker Daltonics) equipped with an Apollo II electrospray ion source in positive ion mode using the following instrument settings: nebulizer gas N$_2$, 1.4 bar; dry gas N$_2$, 6 L/min, 190°C; capillary, –5000 V; end plate offset, −500 V; funnel 1 RF, 200 Vpp; funnel 2 RF, 200 Vpp; in-source collision-induced dissociation energy, 0 V; hexapole RF, 100 Vpp; quadrupole ion energy, 3 eV; collision gas, N$_2$; collision energy, 7 eV; collision RF 150/350 Vpp (timing 50/50); transfer time, 70 μs; prepulse storage, 5 μs; pulser frequency, 10 kHz; spectra rate, 3 Hz. Internal mass calibration of each analysis was performed by infusion of 20 μL 10 mM lithium formiate in isopropanol/water, 1/1 (v/v), at a gradient time of 10 min using a diverter valve. For fragmentation analyses, precursor ions were selected in Q1 with an isolation width of ± 6 D and fragmented in the collision cell applying collision energy of 30 eV. N$_2$ was used as collision gas. Collision-induced dissociation mass spectra were recorded using the following parameter settings: collision RF 150/350 Vpp (timing 50/50); transfer time, 70 μs; prepulse storage, 5 μs; pulser frequency, 10 kHz; spectra rate, 1.5 Hz.

Synthesis of GS-IAN

See Supplemental Protocol online.

Heterologous Expression of GGP1 and GGP3 and Enzymatic Assays

The coding sequence of *GGP3* was amplified from clone U21128 (ABRC) using primers 5′-AATAACACTCGAGATGGTGGTTATTGAGCAGAAG-3′ and 5′-AATAACAGAATTCTCAACCTTTCAGGAAGTTTTTG-3′ and cloned into the *Escherichia coli* expression vector pRSET-A (Invitrogen) using *Xho*I and *Eco*RI restriction sites. GGP1 and GGP3 were then expressed in *E. coli* BL21(DE3)pLysS and purified as previously described for GGP1 (Geu-Flores et al., 2009). As a control, the same *E. coli* strain carrying the empty

pRSET-A was used. For assays with *ggp1-1 ggp3-1* leaf extracts, 200 mg of leaf material were homogenized in 600 μL 85% methanol and spun down for 20 min at 20,000*g*. The supernatant was passed through a methanol-washed SepPak Light C18 cartridge (Waters), and the cleared extract was evaporated and redissolved in 200 μL water. Enzymatic assays were performed in a final volume of 100 μL at room temperature for 1 h in 20 mM Tris buffer, pH 7.5, supplemented 15 μL redissolved extract and 1 μg of purified His-GGP1, His-GGP3, or protein from the empty vector control. Assays with GS-IAN were performed under similar conditions, except that the reaction mixtures were supplemented with 200 μM GS-IAN instead of leaf extracts. Analysis of the products by LC-MS was performed as previously described for GS-B (Geu-Flores et al., 2009). Accurate mass measurements and fragmentation analysis of the products were performed as described above.

Accession Numbers

Sequence data from this article can be found in the Arabidopsis Genome Initiative or GenBank/EMBL databases under the following accession numbers: At4g30530 (*GGP1*), At4g30540 (*GGP2*), At4g30550 (*GGP3*), At2g23960 (*GGP4*), At2g23970 (*GGP5*), At5g05260 (*CYP79A2*), At4g39950 (*CYP79B2*), At2g22330 (*CYP79B3*), At4g31500 (*CYP83B1*), At2g20610 (*SUR1*), At1g24100 (*UGT74B1*), At1g74100 (*SOT16*), At1g18590 (*SOT17*), At1g74090 (*SOT18*), At3g39940 (*APK2*), At4g23100 (*PAD2/GSH1*), At2g30770 (*CYP71A13*), At1g02930 (*GSTF6*), At4g39640 (*GGT1*), At4g39650 (*GGT2*), At4g29210 (*GGT4*), At5g44070 (*PCS1*), and At3g26830 (*PAD3/CYP71B15*).

Supplemental Data

The following materials are available in the online version of this article.

> **Supplemental Figure 1.** Approximate Location of GGP Genes Relative to Each Other in the *Arabidopsis* Genome.
>
> **Supplemental Figure 2.** Microarray-Based Expression Analysis of the Different *GGP* Family Members in Different Tissues of *Arabidopsis* as Visualized Using Genevestigator.
>
> **Supplemental Figure 3.** Glucosinolate Analysis of Wild-Type and *ggp1-1 ggp3-1* Plants 24 h after Treatment with Either a Mock Solution or a Solution of 250 μM Methyl Jasmonate.
>
> **Supplemental Figure 4.** Extracted Ion Chromatogram from LC-MS Analysis of Wild-Type and *ggp1-1 ggp3-1* Plants Accounting for the Cyclized Cys-Gly Conjugates Related to the Glucosinolate 4-msb.
>
> **Supplemental Table 1.** Amino Acid Identities between the Different GGP Family Members.
>
> **Supplemental Table 2.** Fragmentation Analysis of [M+H]+ Ions of Compounds 1 to 10 Found in Extracts of *ggp1-1/ggp3-1* Plants.
>
> **Supplemental Table 3.** Fragmentation Analysis of [M+H]+ Ions of Compounds 12 to 20 Found in Enzymatic Assays with Extracts of *ggp1-1/ggp3-1* Plants and Recombinant GGP1 or GGP3.
>
> **Supplemental Protocol.** Synthesis of GS-IAN [H-Glu(Cys(IAN)-Gly-OH)-OH].

REFERENCES

Alonso, J.M., et al. (2003). Genome-wide insertional mutagenesis of *Arabidopsis thaliana*. Science **301:** 653–657.

Bednarek, P., Pislewska-Bednarek, M., Svatos, A., Schneider, B., Doubsky, J., Mansurova, M., Humphry, M., Consonni, C., Panstruga, R., Sanchez-Vallet, A., Molina, A., and Schulze-Lefert, P. (2009). A glucosinolate metabolism pathway in living plant cells mediates broad-spectrum antifungal defense. Science **323:** 101–106.

Böttcher, C., Westphal, L., Schmotz, C., Prade, E., Scheel, D., and Glawischnig, E. (2009). The multifunctional enzyme CYP71B15 (PHYTOALEXIN DEFICIENT3) converts cysteine-indole-3-acetonitrile to camalexin in the indole-3-acetonitrile metabolic network of *Arabidopsis thaliana*. Plant Cell **21:** 1830–1845.

Brown, P.D., Tokuhisa, J.G., Reichelt, M., and Gershenzon, J. (2003). Variation of glucosinolate accumulation among different organs and developmental stages of *Arabidopsis thaliana*. Phytochemistry **62:** 471–481.

Caissard, J.C., Guivarc'h, A., Rembur, J., Azmi, A., and Chriqui, D. (1994). Spurious localizations of diX-indigo microcrystals generated by the histochemical GUS assay. Transgenic Res. **3:** 176–181.

Chen, S., Glawischnig, E., Jørgensen, K., Naur, P., Jørgensen, B., Olsen, C.E., Hansen, C.H., Rasmussen, H., Pickett, J.A., and Halkier, B.A. (2003). CYP79F1 and CYP79F2 have distinct functions in the biosynthesis of aliphatic glucosinolates in Arabidopsis. Plant J. **33:** 923–937.

Chytilova, E., Macas, J., and Galbraith, D.W. (1999). Green fluorescent protein targeted to the nucleus, a transgenic phenotype useful for studies in plant biology. Ann. Bot. (Lond.) **83:** 645–654.

Clay, N.K., Adio, A.M., Denoux, C., Jander, G., and Ausubel, F.M. (2009). Glucosinolate metabolites required for an *Arabidopsis* innate immune response. Science **323:** 95–101.

Cobbett, C.S. (2000). Phytochelatins and their roles in heavy metal detoxification. Plant Physiol. **123:** 825–832.

Cummins, I., Dixon, D.P., Freitag-Pohl, S., Skipsey, M., and Edwards, R. (2011). Multiple roles for plant glutathione transferases in xenobiotic detoxification. Drug Metab. Rev. **43:** 266–280.

Dixon, D.P., Skipsey, M., and Edwards, R. (2010). Roles for glutathione transferases in plant secondary metabolism. Phytochemistry **71:** 338–350.

Fahey, J.W., Zalcmann, A.T., and Talalay, P. (2001). The chemical diversity and distribution of glucosinolates and isothiocyanates among plants. Phytochemistry **56:** 5–51.

Ganguli, D., Kumar, C., and Bachhawat, A.K. (2007). The alternative pathway of glutathione degradation is mediated by a novel protein complex involving three new genes in *Saccharomyces cerevisiae*. Genetics **175:** 1137–1151.

Gasper, A.V., Al-Janobi, A., Smith, J.A., Bacon, J.R., Fortun, P., Atherton, C., Taylor, M.A., Hawkey, C.J., Barrett, D.A., and Mithen, R.F. (2005). Glutathione S-transferase M1 polymorphism and metabolism of sulforaphane from standard and high-glucosinolate broccoli. Am. J. Clin. Nutr. **82:** 1283–1291.

Geu-Flores, F., Nielsen, M.T., Nafisi, M., Møldrup, M.E., Olsen, C.E., Motawia, M.S., and Halkier, B.A. (2009). Glucosinolate engineering identifies a gamma-glutamyl peptidase. Nat. Chem. Biol. **5:** 575–577.

Glawischnig, E., Hansen, B.G., Olsen, C.E., and Halkier, B.A. (2004). Camalexin is synthesized from indole-3-acetaldoxime, a key branching point between primary and secondary metabolism in Arabidopsis. Proc. Natl. Acad. Sci. USA **101:** 8245–8250.

Grubb, C.D., Zipp, B.J., Ludwig-Müller, J., Masuno, M.N., Molinski, T.F., and Abel, S. (2004). Arabidopsis glucosyltransferase UGT74B1 functions in glucosinolate biosynthesis and auxin homeostasis. Plant J. **40:** 893–908.

Grzam, A., Tennstedt, P., Clemens, S., Hell, R., and Meyer, A.J. (2006). Vacuolar sequestration of glutathione S-conjugates outcompetes a possible degradation of the glutathione moiety by phytochelatin synthase. FEBS Lett. **580:** 6384–6390.

Hansen, B.G., Kliebenstein, D.J., and Halkier, B.A. (2007). Identification of a flavin-monooxygenase as the S-oxygenating enzyme in aliphatic glucosinolate biosynthesis in Arabidopsis. Plant J. **50:** 902–910.

Hayes, J.D., Kelleher, M.O., and Eggleston, I.M. (2008). The cancer chemopreventive actions of phytochemicals derived from glucosinolates. Eur. J. Nutr. **47**(Suppl. 2): 73–88.

Hemm, M.R., Ruegger, M.O., and Chapple, C. (2003). The *Arabidopsis ref2* mutant is defective in the gene encoding CYP83A1 and shows both phenylpropanoid and glucosinolate phenotypes. Plant Cell **15:** 179–194.

Higdon, J.V., Delage, B., Williams, D.E., and Dashwood, R.H. (2007). Cruciferous vegetables and human cancer risk: epidemiologic evidence and mechanistic basis. Pharmacol. Res. **55:** 224–236.

Hopkins, R.J., van Dam, N.M., and van Loon, J.J.A. (2009). Role of glucosinolates in insect-plant relationships and multitrophic interactions. Annu. Rev. Entomol. **54:** 57–83.

Klein, M., Reichelt, M., Gershenzon, J., and Papenbrock, J. (2006). The three desulfoglucosinolate sulfotransferase proteins in Arabidopsis have different substrate specificities and are differentially expressed. FEBS J. **273:** 122–136.

Kliebenstein, D.J., Kroymann, J., Brown, P., Figuth, A., Pedersen, D., Gershenzon, J., and Mitchell-Olds, T. (2001). Genetic control of natural variation in Arabidopsis glucosinolate accumulation. Plant Physiol. **126:** 811–825.

Kurihara, S., Oda, S., Kato, K., Kim, H.G., Koyanagi, T., Kumagai, H., and Suzuki, H. (2005). A novel putrescine utilization pathway involves gamma-glutamylated intermediates of *Escherichia coli* K-12. J. Biol. Chem. **280:** 4602–4608.

Kurihara, S., Oda, S., Kumagai, H., and Suzuki, H. (2006). Gamma-glutamyl-gamma-aminobutyrate hydrolase in the putrescine utilization pathway of *Escherichia coli* K-12. FEMS Microbiol. Lett. **256:** 318–323.

Kusnierczyk, A., Winge, P., Midelfart, H., Armbruster, W.S., Rossiter, J.T., and Bones, A.M. (2007). Transcriptional responses of *Arabidopsis thaliana* ecotypes with different glucosinolate profiles after attack by polyphagous *Myzus persicae* and oligophagous *Brevicoryne brassicae*. J. Exp. Bot. **58:** 2537–2552.

Martin, M.N., Saladores, P.H., Lambert, E., Hudson, A.O., and Leustek, T. (2007). Localization of members of the gamma-glutamyl transpeptidase family identifies sites of glutathione and glutathione S-conjugate hydrolysis. Plant Physiol. **144:** 1715–1732.

Meyer, A.J. (2008). The integration of glutathione homeostasis and redox signaling. J. Plant Physiol. **165:** 1390–1403.

Mikkelsen, M.D., Hansen, C.H., Wittstock, U., and Halkier, B.A. (2000). Cytochrome P450 CYP79B2 from Arabidopsis catalyzes the conversion of tryptophan to indole-3-acetaldoxime, a precursor of indole glucosinolates and indole-3-acetic acid. J. Biol. Chem. 275: 33712–33717.

Mouilleron, S., and Golinelli-Pimpaneau, B. (2007). Conformational changes in ammonia-channeling glutamine amidotransferases. Curr. Opin. Struct. Biol. 17: 653–664.

Møldrup, M.E., Geu-Flores, F., Olsen, C.E., and Halkier, B.A. (2011). Modulation of sulfur metabolism enables efficient glucosinolate engineering. BMC Biotechnol. 11: 12.

Nafisi, M., Goregaoker, S., Botanga, C.J., Glawischnig, E., Olsen, C.E., Halkier, B.A., and Glazebrook, J. (2007). Arabidopsis cytochrome P450 monooxygenase 71A13 catalyzes the conversion of indole-3-acetaldoxime in camalexin synthesis. Plant Cell 19: 2039–2052.

Nagai, T., Ibata, K., Park, E.S., Kubota, M., Mikoshiba, K., and Miyawaki, A. (2002). A variant of yellow fluorescent protein with fast and efficient maturation for cell-biological applications. Nat. Biotechnol. 20: 87–90.

Noctor, G., and Foyer, C.H. (1998). Ascorbate and glutathione: Keeping active oxygen under control. Annu. Rev. Plant Physiol. Plant Mol. Biol. 49: 249–279.

Nour-Eldin, H.H., Geu-Flores, F., and Halkier, B.A. (2010). USER cloning and USER fusion: The ideal cloning techniques for small and big laboratories. Methods Mol. Biol. 643: 185–200.

Nour-Eldin, H.H., Hansen, B.G., Nørholm, M.H.H., Jensen, J.K., and Halkier, B.A. (2006). Advancing uracil-excision based cloning towards an ideal technique for cloning PCR fragments. Nucleic Acids Res. 34: e122.

Ohkama-Ohtsu, N., Radwan, S., Peterson, A., Zhao, P., Badr, A.F., Xiang, C., and Oliver, D.J. (2007a). Characterization of the extracellular gamma-glutamyl transpeptidases, GGT1 and GGT2, in Arabidopsis. Plant J. 49: 865–877.

Ohkama-Ohtsu, N., Zhao, P., Xiang, C., and Oliver, D.J. (2007b). Glutathione conjugates in the vacuole are degraded by gamma-glutamyl transpeptidase GGT3 in Arabidopsis. Plant J. 49: 878–888.

Ossowski, S., Schwab, R., and Weigel, D. (2008). Gene silencing in plants using artificial microRNAs and other small RNAs. Plant J. 53: 674–690.

Pal, R., and Rai, J.P.N. (2010). Phytochelatins: Peptides involved in heavy metal detoxification. Appl. Biochem. Biotechnol. 160: 945–963.

Parisy, V., Poinssot, B., Owsianowski, L., Buchala, A., Glazebrook, J., and Mauch, F. (2007). Identification of PAD2 as a gamma-glutamylcysteine synthetase highlights the importance of glutathione in disease resistance of Arabidopsis. Plant J. 49: 159–172.

Rauhut, T., and Glawischnig, E. (2009). Evolution of camalexin and structurally related indolic compounds. Phytochemistry 70: 1638–1644.

Rea, P.A. (2007). Plant ATP-binding cassette transporters. Annu. Rev. Plant Biol. 58: 347–375.

Reintanz, B., Lehnen, M., Reichelt, M., Gershenzon, J., Kowalczyk, M., Sandberg, G., Godde, M., Uhl, R., and Palme, K. (2001). Bus, a bushy Arabidopsis CYP79F1 knockout mutant with abolished synthesis of short-chain aliphatic glucosinolates. Plant Cell 13: 351–367.

Rosso, M.G., Li, Y., Strizhov, N., Reiss, B., Dekker, K., and Weisshaar, B. (2003). An Arabidopsis thaliana T-DNA mutagenized population (GABI-Kat) for flanking sequence tag-based reverse genetics. Plant Mol. Biol. 53: 247–259.

Rouhier, N., Lemaire, S.D., and Jacquot, J.P. (2008). The role of glutathione in photosynthetic organisms: Emerging functions for gluta-redoxins and glutathionylation. Annu. Rev. Plant Biol. 59: 143–166.

Schlaeppi, K., Bodenhausen, N., Buchala, A., Mauch, F., and Reymond, P. (2008). The glutathione-deficient mutant pad2-1 accumulates lower amounts of glucosinolates and is more susceptible to the insect herbivore Spodoptera littoralis. Plant J. 55: 774–786.

Schuhegger, R., Nafisi, M., Mansourova, M., Petersen, B.L., Olsen, C.E., Svatos, A., Halkier, B.A., and Glawischnig, E. (2006). CYP71B15 (PAD3) catalyzes the final step in camalexin biosynthesis. Plant Physiol. 141: 1248–1254.

Schuler, M.A., and Werck-Reichhart, D. (2003). Functional genomics of P450s. Annu. Rev. Plant Biol. 54: 629–667.

Schwimmer, S., and Kjaer, A. (1960). Purification and specificity of the C-S-lyase of Albizzia lophanta. Biochim. Biophys. Acta 42: 316–324.

Su, T., Xu, J., Li, Y., Lei, L., Zhao, L., Yang, H., Feng, J., Liu, G., and Ren, D. (2011). Glutathione-indole-3-acetonitrile is required for camalexin biosynthesis in Arabidopsis thaliana. Plant Cell 23: 364–380.

Sønderby, I.E., Geu-Flores, F., and Halkier, B.A. (2010). Biosynthesis of glucosinolates—Gene discovery and beyond. Trends Plant Sci. 15: 283–290.

Tantikanjana, T., Mikkelsen, M.D., Hussain, M., Halkier, B.A., and Sundaresan, V. (2004). Functional analysis of the tandem-duplicated P450 genes SPS/BUS/CYP79F1 and CYP79F2 in glucosinolate biosynthesis and plant development by Ds transposition-generated double mutants. Plant Physiol. 135: 840–848.

Tantikanjana, T., Yong, J.W., Letham, D.S., Griffith, M., Hussain, M., Ljung, K., Sandberg, G., and Sundaresan, V. (2001). Control of axillary bud initiation and shoot architecture in Arabidopsis through the SUPERSHOOT gene. Genes Dev. 15: 1577–1588.

Voinnet, O., Rivas, S., Mestre, P., and Baulcombe, D. (2003). An enhanced transient expression system in plants based on suppression of gene silencing by the p19 protein of tomato bushy stunt virus. Plant J. 33: 949–956.

Wu, F.H., Shen, S.C., Lee, L.Y., Lee, S.H., Chan, M.T., and Lin, C.S. (2009). Tape-Arabidopsis Sandwich - A simpler Arabidopsis protoplast isolation method. Plant Methods 5: 16.